

This work was written as part of one of the author's official duties as an Employee of the United States Government and is therefore a work of the United States Government. In accordance with 17 U.S.C. 105, no copyright protection is available for such works under U.S. Law.

Public Domain Mark 1.0

<https://creativecommons.org/publicdomain/mark/1.0/>

Access to this work was provided by the University of Maryland, Baltimore County (UMBC) ScholarWorks@UMBC digital repository on the Maryland Shared Open Access (MD-SOAR) platform.

Please provide feedback

Please support the ScholarWorks@UMBC repository by emailing scholarworks-group@umbc.edu and telling us what having access to this work means to you and why it's important to you. Thank you.

The Response of Stratospheric Constituents to a Solar Eclipse, Sunrise, and Sunset

J. R. HERMAN

NASA/Goddard Space Flight Center, Laboratory for Planetary Atmospheres, Greenbelt, Maryland 20771

The combination of measurements and detailed stratospheric modeling of time-dependent events can be used to confirm chemical mechanisms and their laboratory rate constants or to deduce additional atmospheric properties such as the temperature structure. Sunset, sunrise, and a solar eclipse are events that are characterized by a relatively strong forcing function of brief duration. For these time scales, the detailed time-dependent photochemical and vertical diffusion equations can be solved to predict the variations of minor constituents that are physically important and accessible to current measurement techniques. Careful simultaneous solutions of these equations have shown a significant daytime variation of ozone down to altitudes of about 30 km that can affect the interpretation of spectral absorption type experiments. The calculated sunset variations of [NO] and [HO] show a log linear concentration decay for limited time periods that can be readily converted into atmospheric temperatures by using known reaction rates up to about 70-km altitude. Measurements of the time-dependent behavior of [NO] and [NO₂] during the eclipse of February 26, 1979, are expected to be made from the U2 aircraft at 20-km altitude. If the measurements have sufficient sensitivity, they can be used along with the model predictions to confirm some laboratory chemical rate constants and to estimate the [ClO]/[ClONO₂] ratio at 20-km altitude.

INTRODUCTION

The development and use of detailed numerical models of the upper atmosphere makes it feasible to investigate the time response of atmospheric constituents participating in large photochemical reaction chains. Such models are especially useful for the study of a short-term or transient phenomenon such as a solar eclipse, where the effects of horizontal and vertical transport are relatively small. Density variations that occur during sunrise and sunset present quite different problems both from an experimental and a theoretical point of view. The fundamental differences arise from the abruptness of sunrise at a given wavelength and altitude, with the solar flux driving the photochemistry, in comparison to an equally abrupt sunset, but with the individual chemical decay time constants governing the post sunset chemistry. The time behavior of the solar flux during an eclipse is clearly quite different from either sunrise or sunset. Throughout the eclipse the photochemistry is dominated by the solar flux (except for the few minutes of totality) with a slowly changing solar zenith angle ($\chi < 90^\circ$) in comparison to sunrise-sunset times. Since the time scale for solar flux changes is of the order of an hour, short-lifetime species follow the sun, whereas the concentrations of long-lifetime species are nearly unaffected. Constituents with chemical lifetimes that are substantial fractions of an hour show time lag effects that can be related to specific chemical rate constants.

During the eclipse of February 26, 1979, several different measurements of stratospheric constituent densities and the solar ultraviolet flux are planned, using the high-flying (~20 km) U2 aircraft. Present plans by the several experimenters involved include chemiluminescent detection of NO, NO₂, and O₃ and column density measurements of HNO₃ at 11 μ and of O₃ as part of the UV flux measurements between 200 and 300 nm.

The present paper discusses the expected variations of the above-mentioned species at the 20-km aircraft altitude along with the related photolysis rates. Using the current laboratory cross sections and reaction rates, the variations of [NO] and [NO₂] are related to specific rates and used to deduce the

[ClO]/[ClONO₂] ratio at 20 km. At sunset the atmospheric temperature can be determined from the post sunset decay rate for [NO] and [HO] by using the appropriate laboratory chemical rate constants.

BASIC MODEL DESCRIPTION

The computational model as currently constructed is based on solutions of a diffusion equation for each species:

$$\frac{\partial n_i}{\partial t} + \frac{\partial F_i}{\partial z} = P_i - L_i n_i \quad i = 1, 2, \dots, S$$

$$F_i = -N(z)K(z) \frac{\partial C_i}{\partial z} \quad (1)$$

$$C_i = n_i(z)/N(z)$$

where F_i is the effective mixing flux of the i th species in inverse square centimeters per second, $K(z)$ is the eddy diffusivity, $N(z)$ is the total atmospheric density, $C_i(z)$ is the mixing ratio or fractional concentration, z is the altitude, and t is the time.

$$P_i = \sum_j n_j J_{ij} + \sum_{jk} b_{ijk} n_j n_k + \sum_{jkl} \tau_{ijkl} n_j n_k n_l$$

$$L_i = \sum_j J_{ji} + \sum_{jk} b_{jik} n_k + \sum_{jkl} \tau_{jikl} n_k n_l \quad (2)$$

where J_{ij} is the photolysis rate per second for producing species i and b_{ijk} and τ_{ijkl} are the binary and tertiary reaction rates (cm³s⁻¹ and cm⁶s⁻¹). Tables of these rates are given by Hudson [1977] and by Hampson and Garvin [1977]. All of the approximately 400 reactions given in these references are used that relate to the species listed in the appendix. Three updated rates are used for HO + O₃ = HO₂ + O₂, HO₂ + O₃ = HO + O₂ + O₂, and NO + HO₂ = NO₂ + HO, as listed in Tables 1 and 2.

When scattering is neglected, the J coefficients are computed in the simple manner

$$J_{ij} = \sum_\lambda \sigma_{i\lambda} \Phi_\lambda \exp \left[-\sum_k \sigma_{k\lambda} \int_z^\infty n_k(z') dz' \chi(\lambda) \right] \quad (3)$$

The fluxes Φ_λ are mostly those taken from Ackerman [1971] except in the region around 250 nm, where there is evidence

TABLE 1. Reactions and Rates Contributing to the Production and Loss of O₃ in the Stratosphere

Reaction Number	Reaction	Rate, cm ³ s ⁻¹ , cm ⁶ s ⁻¹
(R1)	O + O ₂ + M = O ₃ + M	K ₂ = 1 × 10 ⁻³⁴ exp (510/T)
(R2)	O + CO ₂ + O ₂ = O ₃ + CO ₂	K ₁₀₀ = 1.3 × 10 ⁻¹⁰
(R3)	O ₃ + hν = O ₂ + O	J ₂ = 1.56 × 10 ⁻⁹
(R4)	O ₃ + hν = O ₂ (¹ Δ) + O(¹ D)	J ₄ = 8.71 × 10 ⁻⁹
(R5)	O + O ₃ = O ₂ + O ₂	K ₃ = 1.9 × 10 ⁻¹¹ exp (-2300/T)
(R6)	O(¹ D) + O ₃ = O ₂ + O + O	K ₁₀₀ = 1.2 × 10 ⁻¹⁰
(R7)	NO + O ₃ = NO ₂ + O ₂	K ₁₁ = 2.3 × 10 ⁻¹² exp (-1450/T)
(R8)	HO + O ₃ = HO ₂ + O ₂	K ₂₁ = 1.8 × 10 ⁻¹² exp (-1000/T)
(R9)	HO ₂ + O ₃ = HO + O ₂ + O ₂	K ₂₂ = 1.4 × 10 ⁻¹⁴ exp (-580/T)
(RA)	H + O ₃ = HO + O ₂	K ₂₀ = 1 × 10 ⁻¹⁰ exp (-516/T)
(RB)	NO ₂ + O ₃ = NO ₃ + O ₂	K ₈₂ = 1.2 × 10 ⁻¹⁹ exp (-2450/T)
(RC)	Cl + O ₃ = ClO + O ₂	K ₈₈ = 2.7 × 10 ⁻¹¹ exp (-257/T)
(RD)	O(¹ D) + O ₃ = O ₂ + O ₂	K ₉ = 1.2 × 10 ⁻¹⁰
(RE)	O ₂ (¹ Δ) + O ₃ = O ₂ + O ₂ + O	K ₁₀₀ = 6 × 10 ⁻¹¹ exp (-2900/T)

Two- and three-body rates are taken from *Hampson and Garvin* [1977]. The *J* coefficients of reactions 3 and 4 are in units of per second and are evaluated at noon and 100-km altitude at equinox. The numbering associated with each reaction corresponds to the curves of Figure 2. Rates *K*₂₁ and *K*₂₂ are from *Ravishankara et al.* [1979] and *Zahnizer and Howard* [1978], respectively.

that the actual fluxes are slightly higher [Simon, 1974]. The absorption cross sections $\sigma_{\lambda, A}$ for each of the 171 wavelength intervals $\Delta\lambda$ are also taken from *Ackerman* [1971] except for the Schumann-Runge band interval of 175–200 nm, where the computations of *Park* [1974] are used. This is important in that it allows the temperature dependence of the O₂ cross sections to cause the appropriate overlapping with the dissociation cross sections $\sigma_{i, D}$ of various constituents (most notably NO and H₂O). *Ch*(χ) is the Chapman function of the solar zenith angle χ computed from the latitude, solar declination, and time according to

$$\cos \chi = \sin (LAT) \sin (DEC) + \cos (LAT) \cos (DEC) \cos (\Omega t + \phi)$$

where Ω is the angular rotation rate of the earth and ϕ is a phase angle for adjusting the zero of time.

When scattering is included, a simple two-stream radiative transfer model based on the matrix operator method of *Plass* [1973] is employed to compute the *J* coefficients. The parameters in this calculation are the single-scattering albedo at each altitude and wavelength $\omega_{\lambda} = \sigma_s / (\sigma_A + \sigma_s)$ and the ground or cloud albedo $\omega_{0\lambda}$ (σ_s is the Rayleigh-scattering cross section, and σ_A is the absorption cross section for each wavelength).

TABLE 2. Reactions and Rates Contributing to the Production and Loss of HO in the Upper Stratosphere and Mesosphere

Reaction	Rate, cm ³ s ⁻¹ , cm ⁶ s ⁻¹
HO ₂ + O ₃ = HO + 2O ₂	K ₂₈ = 1.4 × 10 ⁻¹⁴ exp (-580/T)
NO + HO ₂ = HO + NO ₂	K ₁₁₉ = 3.3 × 10 ⁻¹² exp (245/T)
H + O ₃ = HO + O ₂	K ₂₀ = 1 × 10 ⁻¹⁰ exp (-516/T)
HO ₂ + O = HO + O ₂	K ₂₄ = 3.5 × 10 ⁻¹¹
HO + O ₃ = HO ₂ + O ₂	K ₂₁ = 1.8 × 10 ⁻¹² exp (-1000/T)
HO + O = O ₂ + H	K ₂₂ = 4.2 × 10 ⁻¹¹
HO + HO ₂ = H ₂ O + O ₂	K ₂₅ = 3.0 × 10 ⁻¹¹
HO + H ₂ CO = H ₂ O + HCO	K ₁₂₈ = 3 × 10 ⁻¹¹ exp (-250/T)

Rates *K*₁₁₉ and *K*₂₈ are from *Zahnizer and Howard* [1978], *K*₂₁ is from *Ravishankara et al.* [1979], and the rest are from *Hampson and Garvin* [1977].

The result of including scattering is a modest change in the dissociation rates and in the atmospheric heating rates in some altitude ranges.

Two distinct methods are used to solve the diffusion equations. The first is a linearization procedure where the chemical terms such as $\tau_1 n_1 n_2 n_3$ are expanded in a Taylor series in time to yield

$$\tau_1 n_1 n_2 n_3 \cong -2\tau_1 n_1 n_2 n_3|_0 + \tau_1 [(n_1 n_2)|_0 n_3 + (n_1 n_3)|_0 n_2 + (n_2 n_3)|_0 n_1] \quad (4)$$

The diffusion terms are expanded in central differences, and the time derivative is expanded in a one-sided forward difference.

The resulting fully implicit system of linear equations for each species is solved simultaneously in either steady state mode or the time-dependent mode. This method turns out to be satisfactory in the time-dependent mode but too slowly converging in the approach to steady state. The slow rate of convergence prompted the use of a Newton-Raphson method, as described by *Carnahan et al.* [1969], that necessitates the computation of the Jacobian *J* from the deceptively simple equation

$$\mathbf{n}^{(i+1)} = \mathbf{n}^{(i)} - \mathbf{J}^{-1} \cdot \mathbf{F}^{(i)} \quad (5)$$

$$\mathbf{n} = \mathbf{n}(n_1, n_2, n_3, \dots)$$

where the index *i* is the iteration step and

$$\mathbf{F} = \frac{\partial \mathbf{n}}{\partial t} - \frac{\partial}{\partial z} \left(N(z) K(z) \frac{\partial \mathbf{C}}{\partial z} \right) - \mathbf{P} + \mathbf{L} \mathbf{n} = 0 \quad (6)$$

Care must be taken so that the initial choice of *n* is not too far from the solution. The 'goodness' of the solution is easily checked by the degree to which *F* = 0 in relation to its component parts.

Where possible, the two methods have been compared, and the results are identical if the time step in the linearized method is small enough. The comparison helps to generate reasonable confidence that the solutions are legitimate over a wide range of conditions. Finally, the rate of convergence in steady state and time-dependent modes is quite rapid for the Newton-Raphson technique, which makes it the method of choice for all the calculations carried out in this study.

The obvious complexity of the resulting matrices from either method introduces a considerable opportunity for human error in developing the corresponding computer codes for very large systems of equations. In the present case, more than 60 independent chemically reactive species are integrated. Therefore an automated system was developed that starts with a list of chemical equations in the standard symbolic form *A* + *B* + *C* = *D* + *E* + *F* and its reaction rate and generates the appropriate matrix entries for all terms in the partial differential equations. This means that species can be added or deleted or reactions added or deleted without causing algebraic errors, some of which are virtually undetectable from an examination of the calculated densities. Properly constructed large-scale models are especially prone to this type of error, since the results are always internally self consistent and frequently 'reasonable.'

A common and useful approach to solving the system of equations is to combine certain subsets of the equations into groups (NO_x, Cl_x, HO_x, etc.) by assuming photochemical equilibrium between those members of the group having small chemical time constants with respect to other members. The algebraic elimination of these fast-reaction chains removes the

numerical stiffness problems from the system at the expense of a moderate degree of uncertainty as to the effect of the approximations under various input conditions. Nitric acid is a well-known example of a species that is hard to classify as belonging to one group (HO_x or NO_x). In the steady state mode of operation the degree to which the approximations are valid can easily be assessed. However, in the time-dependent mode the validity of the approximation varies with the time of day or the elapsed time after the onset of a perturbation in the input conditions. For this reason all grouping is avoided, and each species is calculated from its own equation in a simultaneous solution of the entire system.

Boundary conditions are specified for each species at an altitude just above the tropopause and at 100 km as either chemical equilibrium, constant or time-dependent mixing ratio, or as a flux condition. The latter is specified in terms of a three-point one-sided derivative to minimize the error resulting from the use of a coarse altitude grid (up to 5 km). When there is doubt about certain interrelated boundary conditions such as for NO , NO_2 , HNO_3 , etc., the model is extended to the ground, and the appropriate relations are determined for the region above the tropopause.

The basic background atmosphere is calculated from a standard temperature profile taken from the *U.S. Standard Atmosphere* [1976], the assumption of vertical hydrostatic equilibrium, and by assuming a constant mixing ratio for N_2 and O_2 up to 100 km. All other chemical species are independently computed. The eddy diffusivity values are the same as those used by Rundel *et al.* [1978].

In the discussion that follows, the current set of chemical rates are considered to be known. The estimated uncertainties are ignored so that it is possible to obtain some sensitive details of the calculated solutions that can be tested experimentally. The computational problems and solutions presented in this paper will be similar for any 'final' values of the parameters developed in the future. The sensitivity of the photochemical-diffusive solutions to the uncertainties in rates has been thoroughly developed by Rundel *et al.* [1978].

A single set of boundary conditions is adopted at 15-km altitude for all the cases discussed. Some of the key values are 300 ppb of N_2O , 330 ppm of CO_2 , 1.5 ppm of CH_4 , 0.1 ppb of CCl_4 , 1 ppb of CH_2Cl_2 , 0.1 ppb of CFCl_3 (F-11), and 0.1 ppb of CF_2Cl_2 (F-12). The time-dependent calculations are initiated from a steady state solution on the basis of diurnal averages of fluxes [Rundel, 1977] and chemical volume production and loss rates. Averages for each chemical process are computed from the full time dependent solutions and then reused to obtain a new steady state. The steady state solutions are checked for conservation of each atomic species (H, Cl, C, etc.) by direct summation over all the atomic and molecular mixing ratios. The final computations using the time-dependent equations are continued until the solution becomes cyclic in all the species densities. The calculated densities are then treated as data to characterize sunset, sunrise, and an eclipse. For NO and HO their post sunset behavior is interpreted in terms of atmospheric temperature on the basis of the assumption that the chemical processes and their rates are known.

DENSITY VARIATIONS—OZONE

Density variations during an eclipse are smaller than those that occur during sunrise or sunset because of the very short duration of totality and the relatively gradual change in the solar flux in the atmosphere. Sunrise can be characterized as an impulsive event in that the solar photon flux rises many

orders of magnitude during times that are short in relation to most chemical time constants. For each wavelength, sunrise consists of two components: a direct component and a scattered component that dominates until the solar zenith angle is small enough for the atmosphere to be directly illuminated. The impulsive portion of sunrise is associated with the direct illumination. After sunrise the stratosphere is far from chemical equilibrium for times that depend on the species under consideration. Atoms and some radical molecules quickly come to equilibrium with each other and the longer-lived species. The latter may remain significantly out of equilibrium for the better part of a day or longer. Because of this, some of the long-lived species appear to 'ring' after sunrise in response to changes occurring in the densities of other minor constituents.

Ozone is usually considered to be unvarying throughout the day at altitudes below 40 km. The present calculations show that this is not correct to a degree that may be significant for some purposes. From the results shown in Figure 1 the percent variation of ozone is seen to be substantial at altitudes of 30 km and above (8% at 40 km). The various maxima and minima at each altitude are simple displacements in time from the similar features at other altitudes. However, the causes of the maxima and minima are mostly local. That is, the variation in the ozone density at one altitude has only a minor effect on adjacent altitudes through the variation in optical depth. Figure 2 shows the major contributions to the ozone production and loss rates from 0600–0900 hours at 40-km altitude, with the corresponding chemical reactions and rates listed in Table 1. Referring to Figure 2, curves 1 and 2 are the production rates of O_3 and the remaining curves are loss rates. Processes leading to rates smaller than $10^3 \text{ cm}^{-3} \text{ s}^{-1}$ have been omitted from the table but not from the calculations.

The difference between the production and loss rates yields a net loss until about 0730 hours and then a net production until about 1500 hours. Aside from the shifts in time arising from the altitude dependent chemistry rates, the results are the same for all altitudes.

An important consequence arising from the calculated ozone variations is the possible error that may be introduced into some limb-viewing experiments where the ozone absorp-

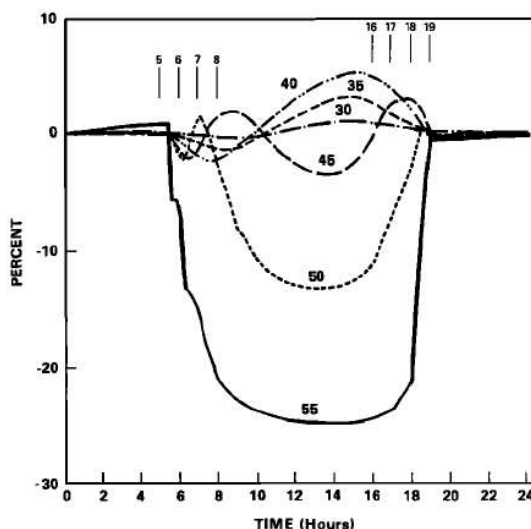


Fig. 1. The percent change time variation of ozone in relation to its midnight value at several altitudes: 30, 35, 40, 45, 50, and 55 km.

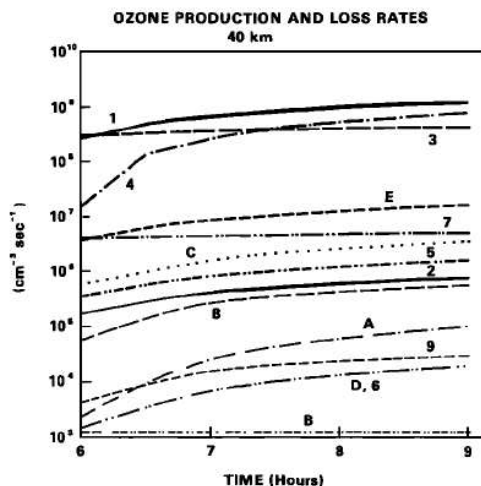


Fig. 2. The ozone production and loss rates at 40 km. Curves 1 and 2 are the production rates and the rest are all loss rates. The time scale is from shortly after sunrise to midmorning (0600–0900 hours). The labels for each curve refer to the chemical reaction set given in Table I.

tion along the line of sight needs to be accurately known. Such experiments are essentially looking through different local times and altitudes. The resulting data may either incorporate a systematic bias or an additional statistical spread, depending on the length of the experimental integration time and the altitudes in the field of view.

The effect of the ozone variation on the other stratospheric constituents is approximately linear with the percentage change in either ozone column content or local concentration. The effect on temperature is approximately $\pm 0.2^\circ\text{K}$ at 40-km altitude, so it only affects those reaction rates with a very strong temperature dependence. For example, a reaction rate with an activation temperature of 10^4 °K would vary by only $\pm 3\%$.

Since the ozone variations under discussion are caused by the smaller terms contributing to the loss process, it is essential that the model calculations are numerically accurate at each time step. Using the data generated at 40 km as an example, the difference between the three major terms, $P(\text{O} + \text{O}_2 + \text{M} = \text{O}_3 + \text{M}) - L(\text{O}_3 + h\nu = \text{O}_2 + \text{O}) - L[\text{O}_3 + h\nu = \text{O}_2(\Delta) + \text{O}(\Delta)]$, is approximately 1% of the production term P , and the sign of the difference is not correlated with $\partial[\text{O}_3]/\partial t$. When all the production and loss terms are included, the correlation is perfect at all times and altitudes. To obtain the desired accuracy, the simultaneous solution for all the constituents at all the altitudes is iterated until the residual error in the solution of each equation is several orders of magnitude smaller than the physical terms of interest. For ozone the worst case residual error is less than 1 part in 10^6 . The other remaining errors arise from the truncation errors in approximating the time and space derivatives. Reducing the step size until no further change can be observed in the resulting solutions between successive trial runs is sufficient to control this source of error. The accuracy and resolution criteria developed to investigate the ozone variation problem are used routinely in the model.

In some recent measurements of ozone concentrations there are indications that there are variations of a few percent at altitudes below 40 km during sunrise and sunset. The most recent evidence of such variations is contained in the data from

a series of balloon flights made between April 1977 and December 1977 [Robbins and Carnes, 1978]. One of these flights shows an increase in $[\text{O}_3]$ at 37 km of 3.6%, commencing at the onset of astronomical twilight and gradually returning to pre-dawn levels about 2.5 hours later. Robbins and Carnes note that their observed ozone increase is contrary to the reduction in the ozone column content above 35 km measured at sunrise by Rigaud [1974]. These measurements need to be done again with more care taken to eliminate the altitude variation of the balloon from the data.

The calculated variation in the ozone column content approximately follows the variation of ozone at 30 km, as shown in Figure 1. A minimum of -0.5% occurs at 0830 hours, and a maximum of $+0.6\%$ at 1500 hours. The variations discussed here are those arising from local effects only, and so represent the minimum change expected during a day in an ideally quiet stratosphere. Even with these conditions data taken by different methods at different times of the day would show a considerable variation. Additional fluctuations might be caused by horizontal transport effects, gravity waves, and the local rising and falling of the atmosphere owing to pressure changes in the air column containing the observation point.

NO AND HO AT SUNSET

Species with moderate to short lifetimes show a very distinctive behavior after sunset in contrast to the sharp, almost featureless response after sunrise. As can be seen in Figures 3, 4, 5, and 6, both $[\text{HO}]$ and $[\text{NO}]$ go from their nighttime values to their daytime values in just a few minutes at all altitudes below about 60 km. Above 60 km the character of the sunrise response is largely determined by the increasing $[\text{O}]/[\text{O}_3]$ ratio. Thus at 80 km, $[\text{NO}]$ is nearly constant throughout the day-night cycle, and $[\text{HO}]$ decreases by an order of magnitude from sunrise to noon.

The post sunset behavior of $[\text{NO}]$ and $[\text{HO}]$ displays a log linear chemical time constant for decay up to about 70 km. The slopes at each altitude can be related to the dominant loss processes. For NO between 30 and 50 km the decay rate is governed by $\text{NO} + \text{O}_3 = \text{NO}_2 + \text{O}_2$, with a reaction rate of $k_{11} = 2.3 \times 10^{-12} \exp(-1450/T)$. For the temperature profile given in the U.S. Standard Atmosphere [1976] table the decay rate time constant is about 22 min at 50 km in comparison to about 4 s at 30 km. At 50 km the second largest decay rate amounts to 18% of the total and is due to $\text{ClO} + \text{NO} = \text{Cl} + \text{NO}_2$ and $\text{HO}_2 + \text{NO} = \text{HO} + \text{NO}_2$. Observations of sunset decay rates for NO could therefore be used to deduce the atmospheric temperature between these two altitudes or to verify the laboratory rate constant k_{11} . In the mesosphere at 70 km only 20% of NO is removed by O_3 at sunset, with most of the rest converted to NO_2 by $\text{HO}_2 + \text{NO} = \text{HO} + \text{NO}_2$ at the rate of $k_{11b} = 3.3 \times 10^{-12} \exp(245/T)$, giving a chemical time constant of about 7 hours. Using the temperature dependence of k_{11b} and the simultaneous measurements of $[\text{NO}]$, $[\text{HO}_2]$, and $[\text{O}_3]$, the determination of the upper atmosphere temperature could be extended to about 70 km. Alternately, knowing any three of the four quantities at two points in time after sunset would permit the fourth to be determined. At 70 km and above, the presence of a nighttime source of NO from the reaction $\text{NO}_2 + \text{O} = \text{NO} + \text{O}_2$ ($k_{10} = 9.1 \times 10^{-12} \text{ cm}^3 \text{ s}^{-1}$) modifies its post sunset behavior. As the production rate increases and becomes comparable to the loss rate, the data may still appear to show a log linear density decay after sunset. However, its interpretation in terms of atmospheric temperature becomes more difficult and uncertain.

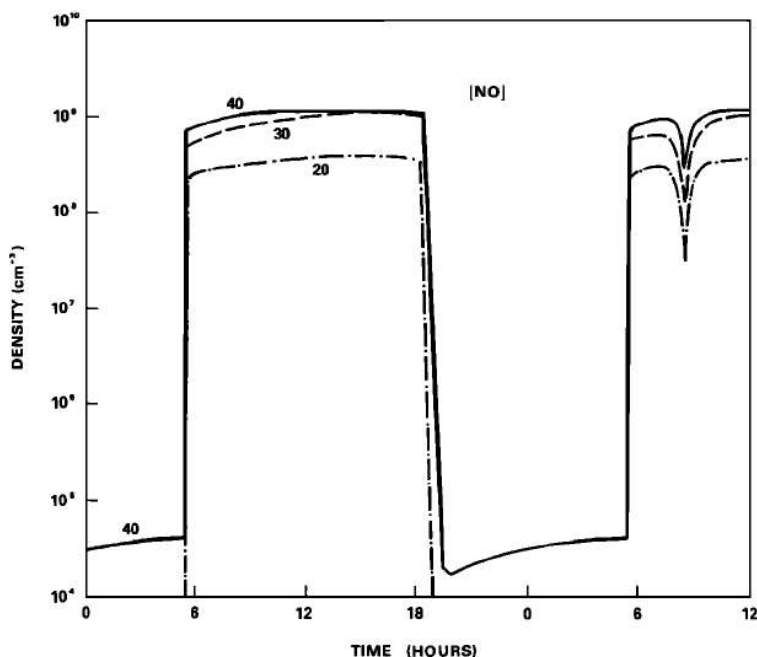


Fig. 3. A 36-hour day-night-day cycle for [NO], including an eclipse at 0830 hours for the altitudes 20, 30, and 40 km.

The similar but more complex behavior of [HO] is shown in Figures 5 and 6. Below 50 km, 90% of the HO is removed by the reaction $\text{HO} + \text{O}_3 = \text{HO}_2 + \text{O}_2$ ($k_{21} = 1.5 \times 10^{-12} \exp(-1000/T)$), with a time constant ranging from about 11 s at 30 km to 5 min at 50 km. For this altitude range, HO can be used in a manner similar to NO if its post sunset log decrement is measured. The measurement has to be made in the short time after sunset when HO is far from chemical equilibrium for a simple interpretation in terms of temperature.

Above 50 km the chemistry becomes increasingly more complex, as does the post sunset behavior of HO. Even for short times after sunset the entire set of reactions given in Table 2 must be considered. At 60 km the dominant reactions are $\text{NO} + \text{HO}_2 = \text{HO} + \text{NO}_2$, $\text{HO} + \text{O}_3 = \text{HO}_2 + \text{O}_2$, and $\text{HO} + \text{H}_2\text{CO} = \text{H}_2\text{O} + \text{HCO}$. Above 60 km, atomic oxygen and atomic hydrogen become increasingly important for the loss and production of nighttime HO. The rates of production and loss are now comparable throughout the night, and the density

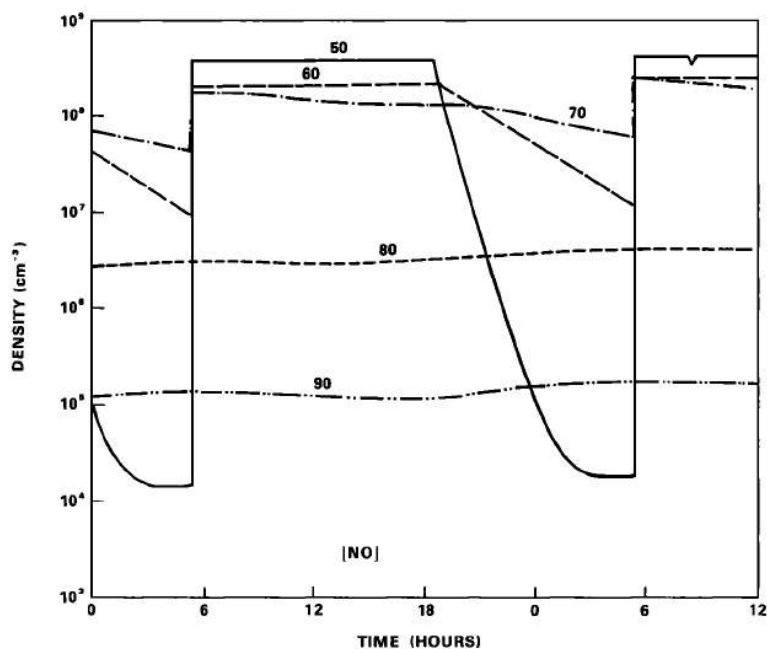


Fig. 4. A 36-hour day-night-day cycle for [NO], including an eclipse at 0830 hours for altitudes 50, 60, 70, 80, and 90 km.

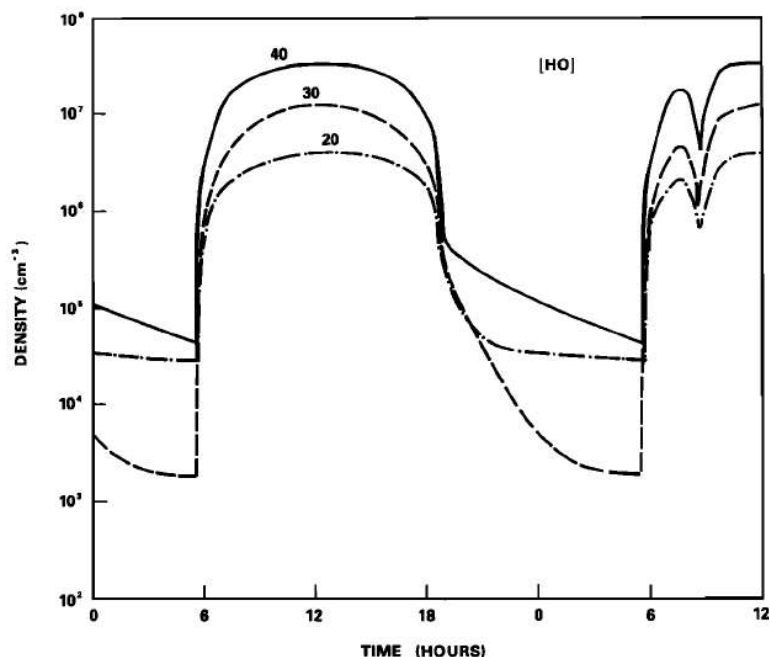


Fig. 5. A 36-hour day-night-day cycle for [HO], including an eclipse at 0830 hours for the altitudes 20, 30, and 40 km.

variations of [HO] can no longer be simply related to a reaction rate and then to atmospheric temperature. Therefore, at altitudes above 50 km a system of at least six chemical rate equations must be solved together for short time periods to relate HO density changes to reaction rates.

Atmospheric measurements to measure the density of HO with adequate sensitivity (at least 10⁴ cm⁻³), time resolution (less than 10 s), and spatial resolution (about 0.5 km) are planned for the near future using the Lidar technique (W. Heaps, private communication, 1978). The success of these

measurements for HO and other species will provide an independent measure of temperature and the verification of rates in several important chemical chains involved in the catalytic destruction of ozone.

STRATOSPHERIC ECLIPSE EFFECTS

Density changes during an eclipse are mainly the result of the slowly varying photolysis rates over a small range of sun angles. The brief period of totality (approximately 3 min for the eclipse of February 26, 1979) in the visible and near-visible

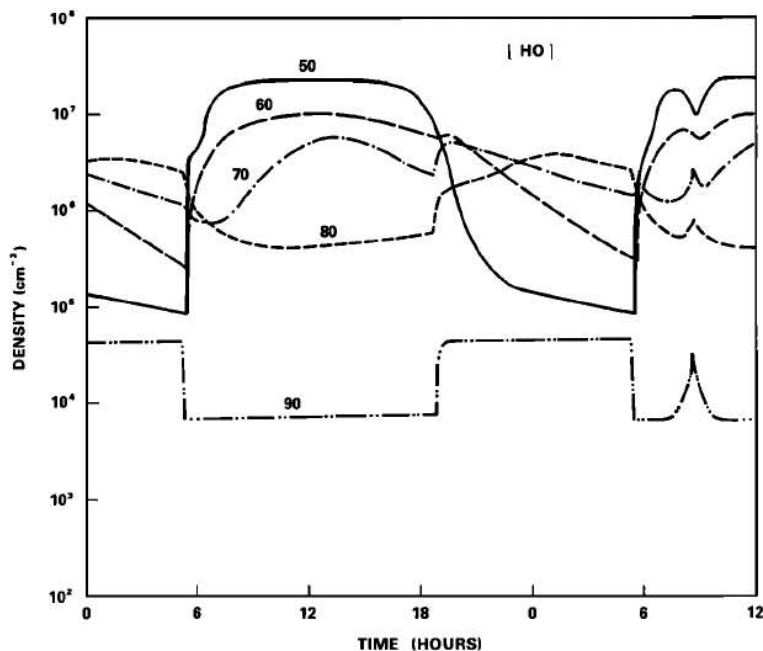


Fig. 6. A 36-hour day-night-day cycle for [HO], including an eclipse at 0830 hours for altitudes 50, 60, 70, 80, and 90 km.

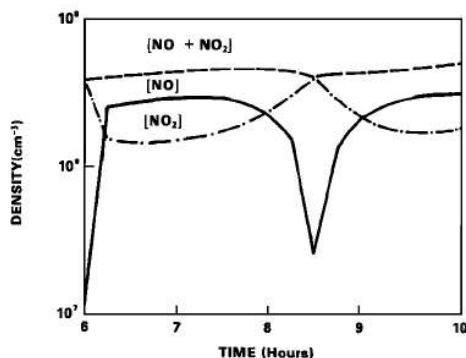


Fig. 7. The variation of [NO], [NO₂], and [NO + NO₂] during a solar eclipse with totality at 0830 hours.

wavelengths produces fractionally large density changes in only the short-lifetime species. During the much longer period of partial obscuration of the sun the atmospheric chemical response to the reduced insolation can easily be observed for many species.

The eclipse is simulated using the timing data contained in the work of Fiala and Lukac [1977]. The basic equation is the fraction of the solar flux that is available from the solar disk during the eclipse as a function of the elapsed time t from first contact:

$$F(t) = 1 - \frac{1}{2\pi} [\arccos A - A(1 - A^2)^{1/2}] \quad (7)$$

$$A = \left| \frac{2t}{T_s} - 1 \right|$$

The total time T_s from first to last contact of the moon with the apparent solar disk is about 2.44 hours along the center of

the path of totality in the vicinity of northern Idaho. The elapsed time t ranges from zero to the time of totality (totality lasts about 2.5 min at 0 km) and ends at $t = T_s$. For $\lambda < 300$ nm the eclipse is not quite total, since the effective size of the solar disk is dependent on the solar temperature where the emission is produced. The UV limb to UV disk intensity ratio ranges from 1 to 10% as the wavelength decreases towards 110 nm [Burton *et al.*, 1967]. This means that the effects of totality are diminished both by the enlarged effective solar disk at UV wavelengths and by atmospheric large-angle Rayleigh scattering over an extended wavelength range.

Totality occurs at about 0830 local time over the North American continent for the eclipse of February 26, 1979. For latitudes along the path of totality, sunrise is about 0650, so the sun will have risen about 20° above the geometric horizon by 0830 when viewed from the ground. First contact at 0710 is quite close to ground sunrise, but by the time totality occurs the eclipse perturbations will be easily distinguishable from sunrise effects.

A number of minor constituents are of considerable interest at 20-km altitude during the eclipse. For some of these (NO, NO₂, HNO₃, O₃, and H₂O), direct measurements can be made of their concentrations from a high-flying aircraft. The chemiluminescent detection of changes in NO and NO₂ should be readily apparent, as illustrated in Figure 7. NO₂ dissociation is mainly by photolysis according to $\text{NO}_2 + h\nu = \text{NO} + \text{O}$. Since this process is dominated by the near-UV (300–400 nm) wavelength region, there is little atmospheric attenuation reducing the photolysis rate even at large solar zenith angles. The principal reactions governing [NO₂] and their percentage contribution to its production and loss rates are shown in Table 3 for 20 km at 0800 hours. As the eclipse progresses toward totality, NO₂ photolysis is continuously reduced, leading to the conversion of NO into NO₂ by the reactions $\text{NO} + \text{O}_3 = \text{NO}_2 + \text{O}_2$

TABLE 3. Reactions and Rates Contributing to the Production and Loss of NO and NO₂ in the Stratosphere

Reaction	Rate, cm ³ s ⁻¹ , cm ³ s ⁻¹	Percent
[NO] Production and Loss		
NO ₂ + $h\nu$ = NO + O	$J_2 = 1.52 \times 10^{-2}$	99.6
HNO ₂ + $h\nu$ = HO + NO	$J_{21} = 4.17 \times 10^{-3}$	0.3
NO ₂ + O = NO + O ₂	$K_{10} = 9.1 \times 10^{-12}$	0.1
NO + O ₃ = NO ₂ + O ₂	$K_{11} = 2.3 \times 10^{-12} \exp(-1450/T)$	81.4
NO + ClO = Cl + NO ₂	$K_{67} = 1 \times 10^{-11} \exp(200/T)$	15.7
NO + HO ₂ = NO ₂ + HO	$K_{110} = 3.3 \times 10^{-12} \exp(245/T)$	2.3
NO + CH ₃ O ₂ = CH ₃ O + NO ₂	$K_{130} = 3.3 \times 10^{-12} \exp(-500/T)$	0.1
NO + HO + M = HNO ₂ + M	$K_{118} = 3.86 \times 10^{-32} \exp(1110/T)$	0.5
[NO₂] Production and Loss		
HNO ₃ + $h\nu$ = HO + NO ₂	$J_7 = 1.68 \times 10^{-4}$	0.1
NO ₃ + $h\nu$ = NO ₂ + O	$J_8 = 2.34 \times 10^{-1}$	0.1
N ₂ O ₅ + $h\nu$ = 2NO ₂ + O	$J_{11} = 6.48 \times 10^{-4}$	0.1
ClNO ₃ + $h\nu$ = ClO + NO ₂	$J_{20} = 1.08 \times 10^{-5}$	0.6
NO + O ₃ = NO ₂ + O ₂	$K_{11} = 2.3 \times 10^{-12} \exp(-1450/T)$	80.8
NO + ClO = Cl + NO ₂	$K_{67} = 1 \times 10^{-11} \exp(200/T)$	15.8
NO + HO ₂ = NO ₂ + HO	$K_{110} = 3.3 \times 10^{-12} \exp(245/T)$	2.4
NO + CH ₃ O ₂ = CH ₃ O + NO ₂	$K_{130} = 3.3 \times 10^{-12} \exp(-500/T)$	0.1
NO ₂ + $h\nu$ = NO + O	$J_2 = 1.52 \times 10^{-2}$	98.5
NO ₂ + O = NO + O ₂	$K_{10} = 9.1 \times 10^{-12}$	0.1
NO ₂ + O ₃ = NO ₃ + O ₂	$K_{22} = 1.2 \times 10^{-13} \exp(-2450/T)$	0.1
NO ₂ + HO + M = HNO ₃ + M	K_{29} = pressure dependent	0.1
NO ₂ + HO ₂ + M = HO ₂ NO ₂ + M	$K_{121} = 2.1 \times 10^{-31}$	0.1
NO ₂ + ClO + M = ClONO ₂ + M	$K_{189} = 3.7 \times 10^{-33} \exp(1150/T)$	1.1

The percentages are for the production and loss of NO and NO₂ separately, computed at 0800 hours during the eclipse. The photolysis rates (J coefficients) are for the same conditions as Table 1 and not those calculated at 0800 hours. Rate K_{118} is from Zahnle and Howard [1978] and the rest are from Hampson and Garvin [1977].

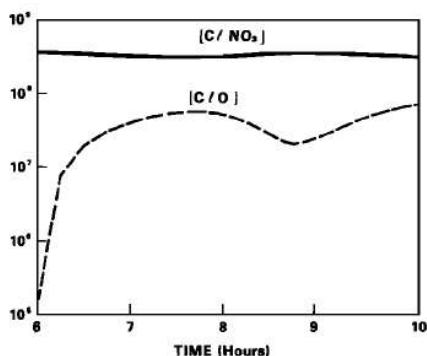


Fig. 8. The variation of $[\text{CINO}_3]$ and $[\text{CIO}]$ during a solar eclipse with totality at 0830 hours.

and $\text{NO} + \text{CIO} = \text{Cl} + \text{NO}_2$. As totality is approached, the CIO channel becomes less important, since $[\text{CIO}]$ also decreases during the eclipse, while $[\text{O}_3]$ remains constant. Taking the $[\text{NO}]$ or $[\text{NO}_2]$ data separately permits information to be obtained concerning the major photolysis rate or k_{11} and k_{67} . However, forming $[\text{NO}] + [\text{NO}_2]$ cancels the influence of all the major chemical reactions on the combined time behavior.

If the time rate of change of $[\text{NO} + \text{NO}_2]$ is measured and compared to the calculated results from

$$\begin{aligned} \frac{d}{dt}[\text{NO}_2 + \text{NO}] = & \sum J - k_{118}[\text{NO}][\text{HO}]\text{M} \\ & - k_{20}[\text{NO}_2][\text{HO}]\text{M} - k_{22}[\text{NO}_2]\text{O}_3 \\ & - k_{121}[\text{NO}_2][\text{HO}_2]\text{M} - k_{189}[\text{CIO}][\text{NO}_2]\text{M} \end{aligned} \quad (8)$$

$$\Sigma J = J(\text{HNO}_3) + J(\text{NO}_3) + J(\text{N}_2\text{O}_5) + J(\text{CINO}_3) \\ + J(\text{CINO}_2) + J(\text{HO}_2\text{NO}_2) + J(\text{HNO}_2)$$

the amount of CINO_3 can be estimated, since $k_{189}[\text{CIO}][\text{NO}_2]\text{M}$ and $J(\text{CINO}_3)$ are the largest terms. The data must be accurate enough to reliably determine whether $[\text{NO}_2 + \text{NO}]$ is increasing or decreasing while the sun is in partial eclipse. Calculated data for $[\text{NO}]$, $[\text{NO}_2]$, $[\text{NO} + \text{NO}_2]$, $[\text{CINO}_3]$, and $[\text{CIO}]$ are shown in Figures 7 and 8. The sum curve for $[\text{NO} + \text{NO}_2]$ varies by only a small amount in relation to either the time variation of $[\text{NO}]$ or $[\text{NO}_2]$ taken separately. This means that a quantitative value of the time rate of change of $[\text{NO} + \text{NO}_2]$, as shown in Figure 9, may be difficult to obtain even though the sign of the quantity can be determined. If the $[\text{CIO}]/[\text{CINO}_3]$ ratio is reduced by 20% or more from the calculated values shown in Figure 8, then $[\text{NO} + \text{NO}_2]$ increases during the partial phase of the eclipse because of the zenith angle dependence contained in $J(\text{CINO}_3)$. The negative portion of the curve shown in Figure 9 is then confined to the approximately 2.5 min of totality. Decreases in the $[\text{CIO}]/[\text{CINO}_3]$ ratio can be obtained by reducing $J(\text{CINO}_3)$, increasing k_{189} , or by simply increasing $[\text{CINO}_3]$. Regardless of the means, a 20% decrease in the presently calculated ratio is the lower boundary for detectability by measuring $[\text{NO} + \text{NO}_2]$ during the eclipse. Increasing the ratio increases the variation of the sum curve for $[\text{NO} + \text{NO}_2]$. If the variation observed in the actual eclipse data is large enough to be significant in relation to the experimental errors in the measurements of $[\text{NO}]$ and $[\text{NO}_2]$, then $[\text{CIO}]/[\text{CINO}_3]$ can be calculated from the dominant terms in (8). Exclusive of

possible errors in k_{189} and the photolysis rate of CINO_3 , neglecting all the remaining terms in (8) amounts to about 20% error when $[\text{CINO}_3]$ is about 4 times smaller than the calculated value of $3.6 \times 10^5 \text{ cm}^{-3}$ at 20 km.

Determining the $[\text{CIO}]/[\text{CINO}_3]$ ratio present in the lower stratosphere is important because of its bearing on the catalytic destruction of O_3 by the Cl_x cycle. CIO is an essential link in recycling Cl atoms to interact with O_3 and again produce CIO via $\text{Cl} + \text{O}_3 = \text{CIO} + \text{O}_2$. Examining Figure 2 shows that this reaction is the third most important loss path of O_3 after $[\text{O}_2(^1\Delta)]$ and $[\text{NO}]$ at today's level of Cl input into the stratosphere via natural (for example, CH_2Cl and CCl_4) or man-made (for example, CCl_4 , CF_3Cl , and CF_2Cl_2) sources. Of course, photolysis of O_3 is the largest loss channel, but this path essentially balances the sole large production mechanism for O_3 ($\text{O} + \text{O}_2 + \text{M} = \text{O}_3 + \text{M}$). The balance is close enough so that the remaining net production and the other loss paths modify the O_3 density. A smaller $[\text{CIO}]/[\text{CINO}_3]$ ratio means that Cl is being tied up in CINO_3 , and therefore the number of O_3 molecules destroyed per atom of Cl introduced into the stratosphere is less than for a larger ratio. A significant fraction of the CINO_3 that is formed in the stratosphere diffuses downward into the troposphere, where it contributes to the processes that wash Cl out of the troposphere in the rain.

The variation of $[\text{CIO}]$ shown in Figure 8 has the minimum of CIO displaced from the 0830 totality by about 20 min. This delay is caused by the difference in recovery rates of Cl and NO. At 0850 hours the CIO chemistry (see Table 3) is dominated by (to the 10% level)

$$\begin{aligned} \frac{d}{dt}[\text{CIO}] = & J(\text{CINO}_3) + k_{88}[\text{Cl}][\text{O}_3] - k_{67}[\text{CIO}][\text{NO}] \\ & - k_{189}[\text{CIO}][\text{NO}_2]\text{M} \end{aligned}$$

where the second and third terms are both 10 times larger than the first and fourth terms (13,684, 129,310, 122,760, and 7,901 $\text{cm}^{-3} \text{ s}^{-1}$). A careful examination of the time response of Cl and NO as the sun reappears shows that NO increases substantially faster than Cl. After about 15 min the term $k_{88}[\text{Cl}][\text{O}_3]$ has recovered sufficiently to cause the $[\text{CIO}]$ to form a minimum and then increase. A similar effect occurs during sunset and sunrise but is harder to combine experimentally because of the time separation between events.

The chemical rate equation (see Table 4) controlling the Cl time behavior during the eclipse is

$$\begin{aligned} \frac{d}{dt}[\text{Cl}] = & k_{44}[\text{CIO}][\text{O}] + k_{67}[\text{CIO}][\text{NO}] + k_{259}[\text{CIOO}][\text{M}] \\ & - k_{88}[\text{Cl}][\text{O}_3] - k_{66}[\text{Cl}][\text{O}_2]\text{M} \end{aligned} \quad (9)$$

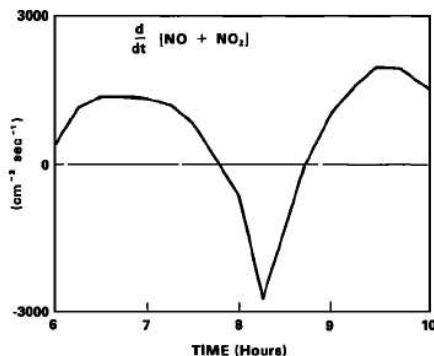


Fig. 9. The value of the time rate of change of $[\text{NO} + \text{NO}_2]$ during a solar eclipse with totality at 0830 hours.

The largest terms, $k_{250}[\text{ClOO}][\text{M}]$ and $k_{60}[\text{Cl}][\text{O}_2]\text{M}$, are in almost perfect balance throughout the eclipse (to within 1 part in 10^6). The next smaller pair, $k_{87}[\text{ClO}][\text{NO}]$ and $k_{60}[\text{Cl}][\text{O}_2]$, is balanced to within about 3 parts in 10^2 . In order for the Cl chemistry to be meaningful the accuracy of solution at each step must be better than 1 part in 10^6 , or the numerical residuals will be comparable to the smaller but controlling chemical terms. These are just the considerations that make grouping of species so attractive even though some physical effects are then altered or missing. Defining chemical families or groups by assuming chemical equilibrium among their members is a good approximation for studying physical effects with time constants that are large in comparison to the largest chemical time constant within a family. For the long-term (years) evaluation of atmospheric perturbations the approximation is excellent, while for times appropriate to sunrise, sunset, or an eclipse the approximations are of limited value. In the present case, if Cl is computed as a member of a Cl_2 family, the offset of the $[\text{ClO}]$ minimum from the time of totality is removed.

SUMMARY

The application of a detailed time-dependent photochemical model to the problem of the stratospheric response to sunrise, sunset, and a solar eclipse has yielded several possibilities for additional experimental measurements. The percent variation of ozone after sunrise is substantial at altitudes of approximately 30 km and above. The variation can amount to a morning to afternoon change of more than 8% at 40 km. This is sufficient to introduce a significant error in some limb-viewing experiments that assume a constant ozone density as a function of local time in the stratosphere.

The time variation of $[\text{NO}]$ and $[\text{HO}]$ at sunrise and sunset has been examined to relate calculated changes in densities to reaction rates and therefore atmospheric temperatures. It is expected that the calculated results can be combined with data for the $[\text{HO}]$ variation after sunset using the Lidar technique to yield information on the main loss channel for HO below about 50 km, $\text{HO} + \text{O}_3 = \text{HO}_2 + \text{O}_2$, and the temperature.

A planned set of measurements during the eclipse of February 26, 1979, from a U2 aircraft at 20-km altitude can be used to investigate portions of the NO_x cycle and its interrelation with the amount of stratospheric ClNO_2 . If the variation of $[\text{NO} + \text{NO}_2]$ can be adequately determined, then the $[\text{ClO}]/$

TABLE 5. Comparison of Model Calculations With Experimental Data

Species	Model	Experimental
$[\text{ClO}]_{50}$	1.3×10^6	$7 \times 10^7, 5 \times 10^6, 8 \times 10^6$
$[\text{Cl}]_{40}$	7.1×10^6	8×10^6
$[\text{HO}]_{50}$	1.2×10^7	1.1×10^7
$\mu(\text{HNO}_3)_{50}$	6	0.8, 3, 7
$\mu(\text{HCl})_{50}$	0.9	1.4
$[\text{NO}_2]/[\text{NO}]_{50}$	1.2	1.6
$[\text{O}_3]_{50}$	3.5×10^{12}	$2.2 \times 10^{12}, 2.8 \times 10^{12}$
$\mu(\text{H}_2\text{O})_{50}$	4.3×10^6	$4.2 \times 10^6 \pm 1.2 \times 10^6$

The experimental data are taken from Hudson [1977]. Species densities $[X]_z$ (in inverse cubic centimeters) or mixing ratios $\mu(X)_z$ (in parts per billion) are given for the indicated species X at the altitude z (in kilometers). Where appropriate a range of experimental values is given.

$[\text{ClNO}_2]$ ratio can be estimated from the photochemical rate equation for $[\text{NO} + \text{NO}_2]$.

APPENDIX: CHEMICAL SPECIES USED IN STRATOSPHERE CHEMISTRY AND DIFFUSION MODEL

A comparison of the model results with experimental data has been made for some of the more important stratospheric species' densities. The comparison was made using a standard set of boundary conditions for the densities but specifying the time of the year, the latitude, and local time appropriate for the experimental data. As shown in Table 5, there is reasonable agreement with the data at fixed local times. The chemical species used in the stratosphere chemistry and diffusion model are: CClO , CCl_2O , CCl_3 , CCl_4 , CCl_2O_2 , CCl_3 , CFCl_2 , CFCl_3 , CF_2Cl , CF_2Cl_2 , CHCl_3 , CH_2 , CH_2Cl , CH_2Cl_2 , CH_3 , CH_3Cl , CH_3O , CH_3OOH , CH_3O_2 , CH_4 , Cl , ClNO , ClNO_2 , ClNO_3 , ClO , ClOO , Cl_2 , CO , CO_2 , C_2H_4 , H , HCl , HCO , HNO_2 , HNO_3 , HO , HOCl , HO_2 , HO_2NO_2 , H_2 , H_2CO , H_2O , H_2O_2 , M , N , NH , NH_2 , NH_3 , NO , NO_2 , NO_3 , N_2 , N_2O , N_2O_5 , $\text{N}(\text{D})$, O , OCIO , O_2 , O_3 , $\text{O}(\text{D})$, $\text{O}(\text{S})$, and $\text{O}_2(\text{D})$.

Acknowledgments. The author would like to thank C. J. McQuillean for the difficult work involved in the programming of the model. Discussions with Richard Stolarski and Dixon Butler were of considerable help throughout the program development.

REFERENCES

- Ackerman, M., Ultraviolet solar radiation related to mesospheric processes, in *Mesospheric Models and Related Experiments*, edited by G. Fiocco, Springer, New York, 1971.
- Burton, W. M., A. Ridgeley, and R. Wilson, *Mon. Notic. Roy. Astron. Soc.*, **135**, 207, 1967.
- Carnahan, B., H. A. Luther, and J. Q. Wilkes, *Applied Numerical Methods*, John Wiley, New York, 1969.
- Fiala, A. D., and M. R. Lukac, Total solar eclipse of 26 February 1979, *Circ. 157*, U.S. Nav. Observ., Washington, D. C., 1977.
- Hampson, R. F., and D. Garvin, Reaction rate and photochemical data for atmospheric chemistry, *Nat. Bur. Stand. Spec. Publ.* **513**, 1977.
- Hudson, R. D., Chlorofluoromethanes and the stratosphere, *NASA Ref. Publ.* **1010**, 1977.
- Park, J. H., The equivalent mean absorption cross sections for the O_2 Schumann-Runge bands: Application to the H_2O and NO photodissociation rates, *J. Atmos. Sci.*, **31**, 1839-1897, 1974.
- Plass, G. N., G. W. Kattawar, and F. E. Catchings, Matrix operator theory of radiative transfer, I, Rayleigh scattering, *Appl. Opt.*, **12**, 314-329, 1973.
- Ravishankara, A. R., P. H. Wine, and A. O. Langford, *J. Chem. Phys.*, in press, 1979.
- Rigaud, P., Photodissociation de l'ozone au moment du lever du soleil, entre 40 et 60 km d'altitude, *Ann. Geophys.*, **30**, 319-328, 1974.

TABLE 4. Reactions and Rates Contributing to the Production and Loss of ClO and Cl in the Stratosphere

Reaction	Rate, $\text{cm}^3 \text{s}^{-1}$, $\text{cm}^6 \text{s}^{-1}$
ClO Production and Loss	
$\text{ClNO}_3 + h\nu = \text{ClO} + \text{NO}_2$	$J = 1.08 \times 10^{-9}$
$\text{Cl} + \text{O}_3 = \text{ClO} + \text{O}_2$	$K_{85} = 2.7 \times 10^{-11} \exp(-257/T)$
$\text{ClO} + \text{O} = \text{Cl} + \text{O}_2$	$K_{84} = 7.7 \times 10^{-11} \exp(-130/T)$
$\text{ClO} + \text{NO} = \text{Cl} + \text{NO}_2$	$K_{87} = 1 \times 10^{-11} \exp(200/T)$
$\text{ClO} + \text{HO}_2 = \text{HOCl} + \text{O}_2$	$K_{211} = 2 \times 10^{-13}$
$\text{ClO} + \text{NO}_2 + \text{M} = \text{ClNO}_2 + \text{M}$	$K_{189} = 3.7 \times 10^{-38} \exp(1150/T)$
Cl Production and Loss	
$\text{ClO} + \text{O} = \text{Cl} + \text{O}_2$	$K_{84} = 7.7 \times 10^{-11} \exp(-130/T)$
$\text{HCl} + \text{HO} = \text{Cl} + \text{H}_2\text{O}$	$K_{66} = 3 \times 10^{-12} \exp(-425/T)$
$\text{ClO} + \text{NO} = \text{Cl} + \text{NO}_2$	$K_{87} = 1 \times 10^{-11} \exp(200/T)$
$\text{ClOO} + \text{M} = \text{Cl} + \text{O}_2 + \text{M}$	$K_{289} = 5.8 \times 10^{-9} \exp(-3580/T)$
$\text{Cl} + \text{O}_3 = \text{ClO} + \text{O}_2$	$K_{85} = 2.7 \times 10^{-11} \exp(-257/T)$
$\text{Cl} + \text{O}_3 + \text{M} = \text{ClOO} + \text{M}$	$K_{69} = 1.7 \times 10^{-38}$

Only those reactions that are most important in the lower stratosphere are listed, although a more complete set is included in the calculations. The rates are from Hampson and Garvin [1977].

- Robbins, D. E., and J. G. Carnes, Variations in the upper stratosphere's ozone profile, paper presented at Symposium 511, World Meteorol. Organ., Toronto, Canada, June 26-30, 1978.
- Rundel, R. D., Determination of diurnal average photodissociation rates, *J. Atmos. Sci.*, **34**, 639-641, 1977.
- Rundel, R. D., D. M. Butler, and R. S. Stolarski, Uncertainty propagation in a stratospheric model, 1, Development of a concise stratospheric model, *J. Geophys. Res.*, **83**, 3063-3073, 1978.
- Simon, P., Balloon measurements of solar fluxes between 1960 Å and 2300 Å, in *Third Conference on CIAP*, pp. 137-141, Department of Transportation, Cambridge, Mass., 1974.
- U.S. Standard Atmosphere, *Publ. NOAA-S/T-1562*, U.S. Gov. Print. Office, Washington, D. C., 1976.
- Zahn timer, M., and C. J. Howard, Recent developments in atmospheric HO₂ chemistry, paper presented at the WMO Symposium on the Geophysical Aspects and Consequences of Changes in the Composition of the Stratosphere, World Meteorol. Organ., Toronto, Canada, June, 1978.

(Received December 6, 1978;
revised February 28, 1979;
accepted March 5, 1979.)